A CONSISTENT MODELLING METHODOLOGY FOR SECONDARY SETTLING TANKS: A RELIABLE NUMERICAL METHOD

RAIMUND BÜRGER[A], STEFAN DIEHL[B], SEBASTIAN FARÅS[B], INGMAR NOPENS[C], AND ELENA TORFS[C]

Abstract. The Consistent Modelling Methodology (CMM) for Secondary Settling Tanks (SSTs) [Bürger, Diehl and Nopens, Water Res. 45 (2011) 2247–2260] leads to a partial differential equation (PDE) of non-linear convection-diffusion type for the solids concentration as a function of depth and time. The model PDE includes a flux that depends discontinuously on spatial position modelling hindered settling and bulk flows, a singular source term describing the feed mechanism, a degenerating term accounting for sediment compressibility, and a dispersion term for the turbulence around the feed inlet. In addition, the solution itself is discontinuous. A consistent, reliable and robust numerical method that properly handles these difficulties is derived and presented in detail. Many constitutive relations for hindered settling, compression and dispersion can be used within the model, allowing the user to switch on and off effects of interest. The method is based on a sound layer-wise spatial discretization and a method-of-lines formulation, which eventually gives rise to a fully discrete numerical scheme. Simulations show the effect of the dispersion term on effluent suspended solids and total sludge mass in the SST.

Keywords: wastewater treatment, continuous sedimentation, secondary clarifier, simulation model, partial differential equation

Nomenclature

A	cross-sectional area of SST [m^2]
B	depth of thickening zone [m]
C	concentration [kg/m^3]
$\hat{C}$	maximum point of f_{bk} [kg/m^3]
C_c	critical concentration [kg/m^3]
C_j	concentration in layer j (3.1) [kg/m^3]
C_{max}	maximum concentration [kg/m^3]
C_{min}	parameter in double-exponential settling velocity function (2.7) [kg/m^3]
D	primitive of d_{comp} (3.2) [kg/(ms)]
$\tilde{D}$	approximate value of D [kg/(ms)]

Date: January 18, 2012.

[A]CI^{2}MA and Departamento de Ingeniería Matemática, Facultad de Ciencias Físicas y Matemáticas, Universidad de Concepción, Casilla 160-C, Concepción, Chile. E-Mail: rburger@ing-mat.udec.cl.

[B]Centre for Mathematical Sciences, Lund University, P.O. Box 118, S-221 00 Lund, Sweden. E-Mail: diehl@maths.lth.se, faras@maths.lth.se.

[C]BIOMATH, Department of Department of Mathematical Modelling, Statistics and Bioinformatics, Coupure Links 653, B-9000 Gent, Belgium. E-Mail: ingmar.nopens@ugent.be, elena.torfs@ugent.be.

F	(convective) flux function [kg/(m^{2}s)]
G	Godunov numerical flux (3.6) [kg/(m^{2}s)]
H	height of clarification zone [m]
J_{comp}	compressive flux (3.4) [kg/(m^{2}s)]
J_{disp}	dispersive flux (3.3) [kg/(m^{2}s)]
M	parameter controlling discretization of C-axis (3.10)
N	number of layers of SST [−]
Q	volumetric flow rate [m^3/s]
S	Stenstrom numerical flux (4.1) [kg/(m^{2}s)]
d_{comp}	compression function (2.8) [m^2/s]
d_{disp}	dispersion function (2.13) [m^2/s]
f_{bk}	Kynch batch flux density function (2.4) [kg/(m^{2}s)]
g	acceleration of gravity [m/s^2]
i	index of concentrations along C-axis
j	layer index [−]
k	parameter in effective solids stress function (2.11) [−]
r_{p}	parameter in double-exponential settling velocity function (2.7) [m^3/kg]
r_{h}	parameter in double-exponential settling velocity function (2.7) [m^3/kg]
r_{V}	parameter in Vesilind hindered settling function (2.6) [m^3/kg]
t	time [s]
v_0	settling velocity of a single particle in unbounded fluid [m/s]
$\tilde{v}_0$	parameter in double-exponential settling velocity function (2.7) [m/s]
v_{hs}	hindered settling velocity
z	depth from feed level in SST [m]

Greek letters.

ΔC	stepsize of discretization of C-axis (3.10) [kg/m^3]
Δt	time step of numerical method [s]
Δz	layer width of numerical method [m]
Φ	(total) flux (2.2) [kg/(m^{2}s)]
α	parameter in effective solid stress function (2.10) [Pa]
α_1	parameter in dispersion coefficient (2.14) [m^{-1}]
α_2	parameter in dispersion coefficient (2.14) [s/m^2]
β	parameter in effective solid stress function (2.10) [kg/m^3]
γ	characteristic function (2.5), equals 1 inside and 0 outside SST
δ	Dirac delta distribution [m^{-1}]
ρ_{f}	density of fluid [kg/m^3]
ρ_{s}	density of solids [kg/m^3]
σ_0	parameter in effective solid stress function (2.11) [Pa]
σ_{e}	effective solid stress [Pa]

Subscripts.

e	effluent

f	feed
u	underflow

Superscripts.

num	numerical (convective, compressive or dispersive) flux function

1. Introduction

1.1. **Scope.** In a recent paper (Bürger et al., 2011) the authors advanced a consistent modelling methodology (CMM) for the simulation of secondary settling tanks (SSTs) in wastewater treatment (WWT). The CMM is based on the conservation of mass and can be cast into the following one-dimensional (1D) partial differential equation (PDE) of nonlinear convection-diffusion type for the solids concentration C as a function of depth z and time t:

$$\begin{aligned} &\frac{\partial C}{\partial t} + \frac{\partial}{\partial z} F(C,z,t) \\ &= \frac{\partial}{\partial z}\left(\left\{ \gamma(z) d_{\mathrm{comp}}(C) + d_{\mathrm{disp}}(z, Q_{\mathrm{f}}(t)) \right\} \frac{\partial C}{\partial z} \right) \\ &\quad + \frac{Q_{\mathrm{f}}(t) C_{\mathrm{f}}(t)}{A} \delta(z). \end{aligned} \tag{1.1}$$

The second term on the left-hand side models hindered settling combined with transport by bulk flows that diverge due to feed, underflow and overflow operations. The expression in curled brackets models sediment compressibility and dispersion, and finally, there is a singular source term modelling the feed mechanism. The different coefficient functions are given in later parts of the paper. The numerical solution of Equation (1.1) is difficult, and cannot be handled by standard engineering-mathematics-textbook methods, since the flux $F(C,z,t)$ is a discontinuous function of z, and the compression coefficient $d_{\mathrm{comp}}(C)$ degenerates, i.e., vanishes over a range of concentration values. These assumptions are intrinsic to 1D SST models.

Since discontinuities may appear in the solution $C = C(z,t)$ of (1.1), this PDE cannot be interpreted in the classical pointwise sense. Instead, it has to be interpreted in the weak sense. Therefore, the conservation law written in integral form in space is a suitable starting point for deriving numerical methods since for any numerical simulation, one has to discretize the model, i.e. compute the concentration only at a finite number of layers of the SST and at discrete time points. Besides the conservation law, discontinuities in the solution should satisfy another physical principle, namely a so-called entropy condition.

It is the purpose of this contribution to launch a numerical method for simulation of SSTs, which is consistent, reliable and robust. *Consistency* requires that the numerical flux (i.e., the flux of the numerical scheme) should approximate the physical flux such that both coincide when discretization parameters tend to zero. A method is said to be *reliable* if the numerical solution is a good approximation of the exact solution of the model PDE. Thus, the numerical method should automatically take the entropy condition into account. Note that consistency alone does *not* ensure reliability. Furthermore, a numerical method is *robust* if it can handle all physically possible initial conditions and input dynamics. In particular,

the method should be able to handle situations far from normal operating conditions, such as storm weather.

The most commonly used simulation method in the WWT community is the one by Takács et al. (1991). For normal operating conditions, it behaves reasonably, but several shortcomings have been reported; see Jeppsson and Diehl (1996a,b), David et al. (2009a), Plósz et al. (2011), Bürger et al. (2011). One feature of the present simulation method is that the numerical flux update can be seen as an extension of that of the Takács method.

A consistent, reliable and robust numerical method for the simulation of clarifier-thickener units has been advanced by Bürger et al. (2005) and used for the simulation of SSTs by De Clercq et al. (2005a, b, 2008). It utilizes the so-called Engquist-Osher numerical flux (Engquist and Osher, 1981). The numerical method presented here is based on the Godunov numerical flux (Godunov, 1959) along with a new algorithm for its computation. This method is slightly less accurate than the Engquist-Osher method, however, it is easier to implement and requires fewer computations, which might be preferable to engineers. We refer to Bürger et al. (2012) for thorough comparisons between these two methods and further discussion. This contribution presents all implementation details necessary to numerically approximate the exact solution of (1.1), and thereby to simulate the response of the SST to various operating conditions. In doing so, we advance a method-of-lines description so that the simulation model could be used in conjunction with ODE (ordinary differential equation) solvers typically used for the biokinetic model equations for the biological reactor.

1.2. **Related work.** The kinematic sedimentation theory (Kynch, 1952) postulates that the solids settling velocity is a function of the local solids concentration only. This turns the conservation of mass equation into a nonlinear, first-order hyperbolic PDE for which a specialized mathematical and numerical theory is necessary. Available SST simulators can roughly be divided into two categories. One contains the traditional layer models where certain rules control the flux between neighbouring layers and/or additional heuristic assumptions have been included directly into the numerical method (Stenstrom, 1976; Attir and Denn, 1978; Vitasovic, 1989; Takács et al., 1991; Otterpohl and Freund, 1992; Härtel and Pöpel, 1992; Koehne et al., 1995; Watts et al., 1996; Chatellier and Audic, 2000; Queinnec and Dochain, 2001; Giokas et al., 2002; Verdickt et al., 2005; Plósz et al., 2007, 2011; Abusam and Keesman, 2009; David et al., 2009a, 2009b; Guo et al., 2010). In the other category, the simulator is derived from the governing PDE (Anderson and Edwards, 1981; Lev et al., 1986; Chancelier et al., 1997; Diehl and Jeppsson, 1998; De Clercq et al., 2003; Wett, 2002; Martin, 2004; Bürger et al., 2005).

In parallel to the development of simulation models, engineering operating charts are used for the prediction and design of SSTs. The construction of such charts have been based on the classical solids flux theory, closely connected to the PDE theory by Kynch (1952). In this theory, compressive and dispersive effects are ignored, which makes it possible to construct exact solutions (Diehl, 1996, 2008).

1.3. **Outline of the paper.** We first recall in Section 2 the mathematical model in detail, where we adhere to the notation of Bürger et al. (2011). In Section 3, we discretize the model. To this end, we first specify (in Sect. 3.1) how the 1D SST is subdivided into computational cells, which we from now on call layers, and formulate the conservation law

for each layer (Sect. 3.2). We then outline in Sections 3.3 and 3.4 the (spatial) discretization of the convective, dispersive and compressive fluxes. This yields a method-of-lines formulation, which is stated in Sect. 3.5, and which consists in one ODE for each layer. We then derive a fully discrete numerical method by introducing (in Sect. 3.6) a time discretization, and explicitly state the restriction of the time step (Sect. 3.7).

Of particular interest is the relation of the Godunov numerical flux with the method by Takács et al. (1991). In fact, it is well known that Takács' method yields incorrect results, for example under wet weather conditions. We demonstrate in Section 4 how to convert an existing implementation of Takács' simulation method into the present method. Simulations and conclusions can be found in Sections 5 and 6, respectively.

2. Mathematical model

Consider an idealized SST outlined in Figure 1. The height of the clarification zone is denoted by H, and the depth of the thickening zone by B. The volumetric flows leaving the SST at the underflow and effluent levels ($z = B$ and $z = -H$, respectively) are denoted by Q_{u} and Q_{e}, respectively, where $Q_{\mathrm{u}}, Q_{\mathrm{e}} \geq 0$. We assume that there is either an upward (Q_{e}) or a downward (Q_{u}) volumetric flow at each point of the downward-pointing z-axis, except for $z = 0$, where the feed source is located. The assumption of one-dimensionality implies that horizontal currents, wall effects, raking, and other features are neglected. Moreover, we assume that the SST is cylindrical with a constant cross-sectional area A (a 1D formulation where A depends on depth z is discussed by Bürger et al. (2010)).

The z-axis can be divided into the effluent zone ($z < -H$), the clarification zone ($-H < z < 0$), the thickening zone ($0 < z < B$), and the underflow zone ($z > B$).

Consider an arbitrary interval of the depth axis: (z_1, z_2). The conservation law of mass states that the increase of mass per time unit in the interval (z_1, z_2) equals the flux in ($\Phi|_{z=z_1}$) minus flux out ($\Phi|_{z=z_2}$) plus the production inside the interval:

$$\frac{\mathrm{d}}{\mathrm{d}t}\int_{z_1}^{z_2} AC(z,t)\,\mathrm{d}z = A\left(\Phi|_{z=z_1} - \Phi|_{z=z_2}\right) + \int_{z_1}^{z_2} Q_{\mathrm{f}}(t)C_{\mathrm{f}}(t)\delta(z)\,\mathrm{d}z, \tag{2.1}$$

where $Q_{\mathrm{f}} = Q_{\mathrm{e}} + Q_{\mathrm{u}}$ is the volumetric feed flow, C_{f} is the feed concentration and

$$\begin{aligned}&\Phi\left(C, \frac{\partial C}{\partial z}, z, t\right)\\ &\quad = F(C,z,t) - \left(\left(\gamma(z)d_{\mathrm{comp}}(C) + d_{\mathrm{disp}}(z, Q_{\mathrm{f}}(t))\right)\frac{\partial C}{\partial z}\right)\end{aligned} \tag{2.2}$$

is the total flux. Here,

$$F(C,z,t) = \begin{cases} -Q_{\mathrm{e}}(t)C/A & \text{for } z < -H,\\ -Q_{\mathrm{e}}(t)C/A + f_{\mathrm{bk}}(C) & \text{for } -H \leq z < 0,\\ Q_{\mathrm{u}}(t)C/A + f_{\mathrm{bk}}(C) & \text{for } 0 < z \leq B,\\ Q_{\mathrm{u}}(t)C/A & \text{for } z > B \end{cases} \tag{2.3}$$

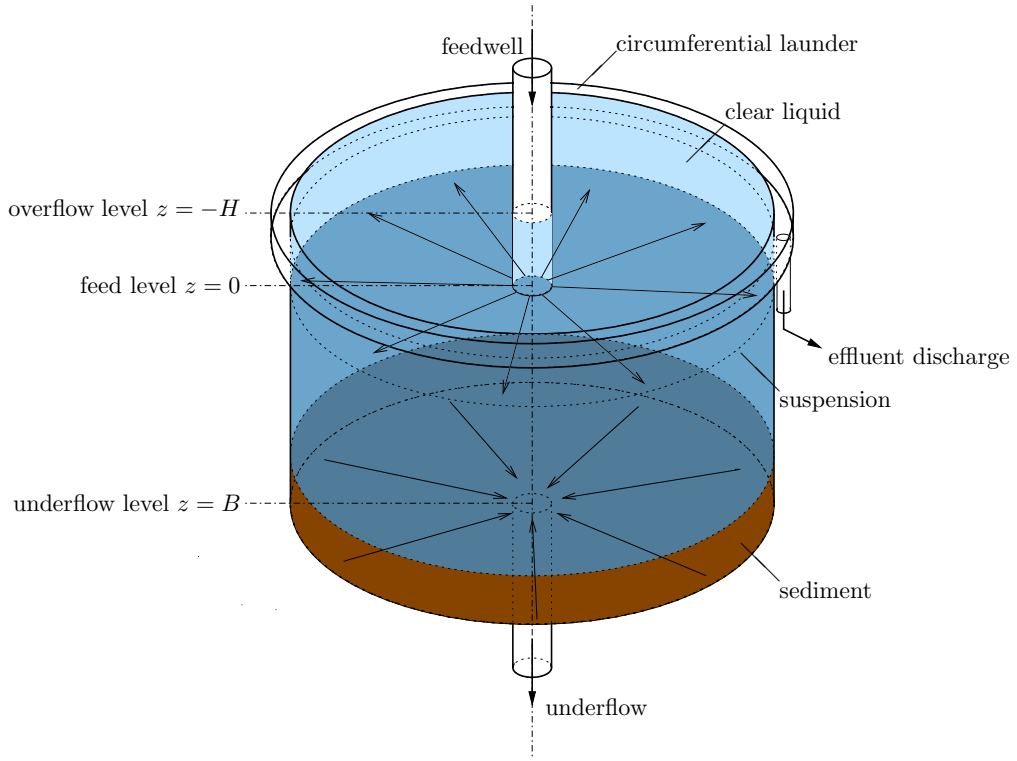

FIGURE 1. Schematic illustration of the SST.

is the convective flux function, which involves the Kynch batch flux density function

$$f_{\rm bk}(C) := Cv_{\rm hs}(C), \tag{2.4}$$

where $v_{\rm hs}(C)$ is the hindered settling velocity (Kynch, 1952). The parameter $\gamma = \gamma(z)$ indicates whether z is a height in the interior or the exterior of the SST, i.e.,

$$\gamma(z) = \begin{cases} 1 & \text{for } -H \le z \le B, \\ 0 & \text{for } z < -H \text{ or } z > B. \end{cases} \tag{2.5}$$

Moreover, $d_{\rm comp} = d_{\rm comp}(C)$ is a concentration-dependent function accounting for sediment compressibility, and $d_{\rm disp} = d_{\rm disp}(z, Q_{\rm f}(t))$ is a dispersion coefficient that incorporates mixing of lower and higher sludge concentrations by "lumping" several mechanisms related to density and turbulent currents together.

We emphasize that Equation (2.1) is the model in integral form. It can be expressed as the PDE (1.1); however, this equation cannot be interpreted pointwise, but only in the so-called weak sense. Note that the model equations (2.1)–(2.3) do not contain the actual cross-sectional areas of the outlet pipes. We are only interested in the concentrations in the outlet pipes and not the bulk velocities. Under the assumption that the particles follow the water streams in the outlet pipes, the concentrations are independent on the sizes of the pipes. For a comprehensive analysis on this, we refer to Diehl (2000).

One choice of $v_{\rm hs}$ common in SST modelling is the hindered settling expression proposed by Vesilind (1968),

$$v_{\rm hs}(C) = v_0 \mathrm{e}^{-r_{\rm V} C}, \tag{2.6}$$

where v_0 is the settling velocity for a single particle and $r_{\rm V} > 0$ is a parameter. Another popular expression is the double exponential function by Takács et al. (1991) (rewritten by Diehl and Jeppsson (1998) so that $v_{\rm hs}(C) \geq 0$):

$$v_{\rm hs}(C) = \max\left\{0, \min\left\{\tilde{v}_0, v_0\big(\mathrm{e}^{-r_{\rm h}(C-C_{\rm min})} - \mathrm{e}^{-r_{\rm p}(C-C_{\rm min})}\big)\right\}\right\}, \tag{2.7}$$

where $\tilde{v}_0$ and v_0 are the maximal practical and theoretical settling velocities, respectively, $r_{\rm h}$ and $r_{\rm p}$ are settling parameters, and $C_{\rm min}$ is the concentration below which $v_{\rm hs} = 0$.

The compression function $d_{\rm comp}$ is given by (Bürger et al., 2005)

$$d_{\rm comp}(C) = \frac{\rho_{\rm s} v_{\rm hs}(C)}{g(\rho_{\rm s} - \rho_{\rm f})} \sigma_{\rm e}'(C) \tag{2.8}$$

where $\rho_{\rm s}$ and $\rho_{\rm f} < \rho_{\rm s}$ are the (constant) solid and fluid mass densities, g is the acceleration of gravity, and $\sigma_{\rm e} = \sigma_{\rm e}(C)$ is the so-called effective solid stress function, which satisfies

$$\sigma_{\rm e}'(C) \begin{cases} = 0 & \text{for } 0 \leq C < C_{\rm c}, \\ > 0 & \text{for } C > C_{\rm c}, \end{cases} \tag{2.9}$$

where $C_{\rm c}$ is a material-dependent critical concentration or gel point at which the solid particles start to physically touch each other, so that solids stress can be transmitted. Common semi-empirical formulas for $\sigma_{\rm e}(C)$ include the function by De Clercq et al. (2008),

$$\sigma_{\rm e}(C) = \begin{cases} 0 & \text{for } C < C_{\rm c}, \\ \alpha \ln\left(1 + \dfrac{C - C_{\rm c}}{\beta}\right) & \text{for } C \geq C_{\rm c}. \end{cases} \tag{2.10}$$

with parameters $\alpha > 0$ and $\beta > 0$, and the power-law-type expression (Tiller and Leu, 1980)

$$\sigma_{\rm e}(C) = \begin{cases} 0 & \text{for } C < C_{\rm c}, \\ \sigma_0\big((C/C_{\rm c})^k - 1\big) & \text{for } C \geq C_{\rm c}. \end{cases} \tag{2.11}$$

with parameters $\sigma_0 > 0$ and $k > 0$. Empirical functions with model parameters have been suggested for $d_{\rm comp}$ directly (Vaccari and Uchrin, 1989; Cacossa and Vaccari, 1994). We prefer, however, the physically motivated formula (2.8), which involves both constitutive relations $v_{\rm hs}$ and $\sigma_{\rm e}$. In the simulations in Section 5, we will use (2.6) and (2.10), which together with the property (2.9) means that

$$d_{\rm comp}(C) = \begin{cases} 0 & \text{for } 0 \leq C < C_{\rm c}, \\ \dfrac{\rho_{\rm s}\alpha v_0 \mathrm{e}^{-r_{\rm V} C}}{g(\rho_{\rm s} - \rho_{\rm f})(\beta + C - C_{\rm c})} & \text{for } C \geq C_{\rm c}. \end{cases} \tag{2.12}$$

The dispersion function $d_{\rm disp}$ is often set as the product of the fluid velocity and some characteristic length scale (Anderson and Edwards, 1981; Lee et al., 2006). For our purpose,

d_{disp} should capture mixing phenomena in three dimensions caused by the feed inlet. It is therefore reasonable to set

$$d_{\mathrm{disp}}\big(z, Q_{\mathrm{f}}(t)\big) = \frac{Q_{\mathrm{f}}(t)}{A} L(z, Q_{\mathrm{f}}(t)),$$

where L is a continuous function, which is zero some distance away from the inlet. Once a portion of suspended sludge has left the SST through one of the outlets, it cannot return. To guarantee that the model captures this property, we restrict the effect of dispersion to the interior of the tank by setting

$$d_{\mathrm{disp}}\big(z, Q_{\mathrm{f}}(t)\big) \begin{cases} = 0 & \text{for } z \leq -H \text{ and } z \geq B, \\ \geq 0 & \text{for } -H < z < B. \end{cases} \tag{2.13}$$

One may use a cosine function:

$$d_{\mathrm{disp}}\big(z, Q_{\mathrm{f}}\big) = \begin{cases} \alpha_1 Q_{\mathrm{f}} \cos\left(\dfrac{\pi z}{2\alpha_2 Q_{\mathrm{f}}}\right) & \text{for } |z| < \alpha_2 Q_{\mathrm{f}}, \\ 0 & \text{for } |z| \geq \alpha_2 Q_{\mathrm{f}}, \end{cases}$$

where α_1 and α_2 are positive parameters (and α_1 contains A). In particular, $\alpha_2 Q_{\mathrm{f}}$ determines the width of the region where dispersion occurs. In view of (2.13), we require that

$$\alpha_2 < \frac{\min(H, B)}{\max_{t \geq 0} Q_{\mathrm{f}}(t)}.$$

An alternative and smooth function is the following:

$$d_{\mathrm{disp}}(z, Q_{\mathrm{f}}) = \begin{cases} \alpha_1 Q_{\mathrm{f}} \exp\left(\dfrac{-z^2/(\alpha_2 Q_{\mathrm{f}})^2}{1 - |z|/(\alpha_2 Q_{\mathrm{f}})}\right) & \text{for } |z| < \alpha_2 Q_{\mathrm{f}}, \\ 0 & \text{for } |z| \geq \alpha_2 Q_{\mathrm{f}}. \end{cases} \tag{2.14}$$

The ingredients d_{comp} and d_{disp} are independent from each other, and are optional in the sense that we may set $d_{\mathrm{comp}} \equiv 0$ or $d_{\mathrm{disp}} \equiv 0$ for materials and SSTs that are not assumed to exhibit sludge compressibility or dispersion, providing high flexibility in model use. In the numerical method to be developed, both options are explicitly included and not lumped like in other proposed methods.

Let us for a moment set $d_{\mathrm{disp}} \equiv 0$ and assume that d_{comp} is given by (2.8). For ease of discussion, consider only the thickening zone, $0 < z < B$. Then (1.1) reduces to

$$\frac{\partial C}{\partial t} + \frac{\partial}{\partial z}\left(f_{\mathrm{bk}}(C) + \frac{Q_{\mathrm{u}}(t)}{A} C\right) = \frac{\partial}{\partial z}\left(d_{\mathrm{comp}}(C) \frac{\partial C}{\partial z}\right). \tag{2.15}$$

In view of (2.8) we see that (2.15) is a first-order conservation law whenever $0 \leq C < C_{\mathrm{c}}$ and a second-order parabolic equation for $C > C_{\mathrm{c}}$. Since (2.15) degenerates to first-order hyperbolic type on a solution interval $[0, C_{\mathrm{c}})$ of positive length, this equation is called *strongly degenerate parabolic*. The location of the type-change interface $C = C_{\mathrm{c}}$, corresponding to the sludge blanket level, is unknown a priori. The numerical method has, however, the property that it is unnecessary to explicitly track this interface. Analogous observations hold, of course, for the full equation (1.1) at any position where $d_{\mathrm{disp}}(z, Q_{\mathrm{f}}(t)) = 0$.

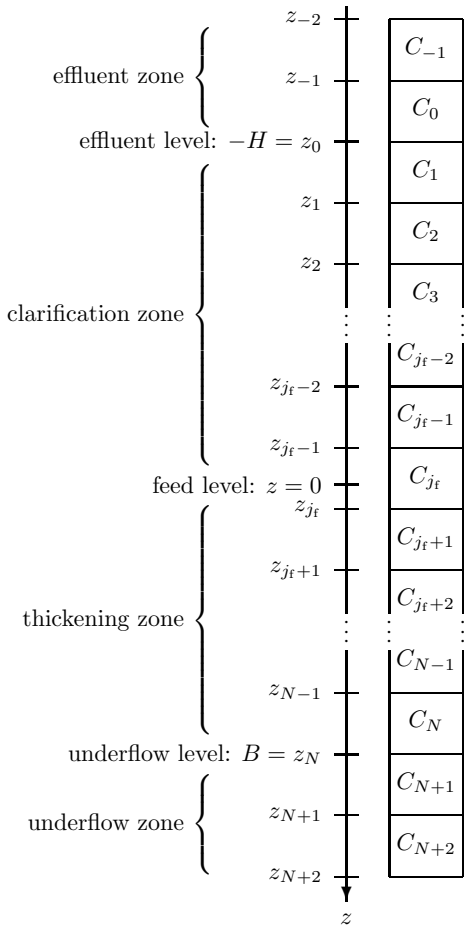

FIGURE 2. Schematic illustration of the subdivision of the computational domain into layers.

Given initial data at $t = 0$, we call the (entropy-satisfying) solution of Equation (1.1), interpreted in the weak sense, the *exact* solution of the model. A numerical solution is always an approximation of the exact solution. No boundary conditions are needed, since (1.1) is defined on the whole real line.

3. Discretization of the mathematical model

3.1. **Subdivision into layers.** We subdivide the tank into N internal layers, so that each layer has the depth $\Delta z = (B + H)/N$. We assume that the boundaries between the layers are located at positions (Figure 2)

$$z_j := j\Delta z - H, \quad j = 0, \dots, N.$$

Thus, the effluent and underflow levels precisely coincide with layer boundaries, i.e., $z_0 = -H$ and $z_N = B$. We will refer to "layer j" as the interval $[z_{j-1}, z_j]$, and adopt further notation correspondingly. Define $j_f := \lceil H/\Delta z \rceil$, which is equal to the smallest integer larger or equal to $H/\Delta z$. Then the feed inlet ($z = 0$) is located in the interval $(z_{j_f-1}, z_{j_f}]$ and the

corresponding layer is called the "feed layer". In the formulation of the numerical scheme we add two layers to both the top and bottom corresponding to the effluent and underflow zones, respectively. Thus, the computational domain is composed of $N + 4$ intervals of length Δz, enclosed by the points z_j, $j = -2, \ldots, N + 2$. These four layers are necessary for a correct numerical implementation. This ingredient differs from most of the published SST simulators, which make the generally erroneous assumption that the concentration is continuous over the outlet locations, i.e., the outlet concentrations are the same as in layer 1 and N, respectively. In the present method, the effluent and underflow concentrations (C_{e} and C_{u}) are those found in layers 0 and $N+1$, respectively. Further discussion on this point can be found in Bürger et al. (2012).

3.2. **The conservation law for each layer.** Motivated by the particular form of the left-hand side of (2.1), we define $C_j = C_j(t)$ as the average of the exact solution C over layer j at time t (see Figure 2):

$$C_j(t) := \frac{1}{\Delta z} \int_{z_{j-1}}^{z_j} C(z,t)\,\mathrm{d}z. \tag{3.1}$$

The numerical method is derived by first rewriting the governing equation (2.1) in a slightly different form. We define the primitive of d_{comp},

$$D(C) := \int_{C_{\mathrm{c}}}^{C} d_{\mathrm{comp}}(s)\,\mathrm{d}s, \tag{3.2}$$

so that we may write

$$d_{\mathrm{comp}}(C)\frac{\partial C}{\partial z} = \frac{\partial}{\partial z} D(C).$$

We can then write the total flux in (2.2) as

$$\Phi = F - J_{\mathrm{disp}} - J_{\mathrm{comp}},$$

where

$$J_{\mathrm{disp}}(z,t) := d_{\mathrm{disp}}\big(z, Q_{\mathrm{f}}(t)\big)\frac{\partial C}{\partial z}, \tag{3.3}$$

$$J_{\mathrm{comp}}(z,t) := \gamma(z)\frac{\partial D(C)}{\partial z}. \tag{3.4}$$

Of course, J_{disp} and J_{comp} are functions of z and t also via the derivatives of $C(z,t)$ and $D(C(z,t))$, however, we choose the easier notation of dependence (z,t). Equation (2.1) can now be rewritten, for each layer j, in the following way by dividing by the constants A

and Δz:

$$\begin{aligned}\frac{\mathrm{d}C_j}{\mathrm{d}t} = &-\frac{F(C(z_j,t),z_j,t) - F(C(z_{j-1},t),z_{j-1},t)}{\Delta z}\\ &+\frac{J_{\mathrm{disp}}(z_j,t) - J_{\mathrm{disp}}(z_{j-1},t)}{\Delta z}\\ &+\frac{J_{\mathrm{comp}}(z_j,t) - J_{\mathrm{comp}}(z_{j-1},t)}{\Delta z}\\ &+\frac{1}{\Delta z}\int_{z_{j-1}}^{z_j}\frac{Q_{\mathrm{f}}(t)C_{\mathrm{f}}(t)}{A}\delta(z)\,\mathrm{d}z.\end{aligned} \tag{3.5}$$

This equation is an exact version of the conservation law. In particular, the finite difference quotient of the convective flux function F (and likewise for J_{disp} and J_{comp}) is not an approximation of a derivative; it is a consequence of the conservation law for a layer.

To convert (3.5) into a numerical scheme, we express the right-hand side of (3.5) in terms of the layer concentration C_j and its neighbours only.

3.3. **Approximation of the convective flux.** The convective flux $F(C(z_j,t),z_j,t)$ in (3.5) at the boundary between layers j and $j+1$ should be replaced by a numerical convective flux F_j^{num} associated with position z_j. Such a numerical flux will in general depend on the adjacent layer concentrations $C_j(t)$ and $C_{j+1}(t)$, i.e.,

$$F_j^{\mathrm{num}}\big(C_j(t),C_{j+1}(t),t\big) \approx F\big(C(z_j,t),z_j,t\big).$$

There are several reasonable choices of the numerical flux F_j^{num}, and several restrictions that must be met to ensure convergence to the exact solution. We have discussed this, compared different numerical methods for the present type of PDE (Bürger et al., 2012) and pointed out some pitfalls.

Since a simulator of the SST should eventually be included in a model of an entire WWT plant, the simulation speed is important. Therefore, we choose here the Godunov numerical flux (Godunov, 1959) on f_{bk} as an approximation of $f_{\mathrm{bk}}(C(z_j,t))$:

$$G_j = G_j(C_j,C_{j+1}) = \begin{cases}\min\limits_{C_j\le C\le C_{j+1}} f_{\mathrm{bk}}(C) & \text{if } C_j \le C_{j+1},\\ \max\limits_{C_j\ge C\ge C_{j+1}} f_{\mathrm{bk}}(C) & \text{if } C_j > C_{j+1}.\end{cases} \tag{3.6}$$

The evaluation of G_j is greatly simplified in the common situation that f_{bk} has precisely one local maximum at a value $\hat{C}$. (For example, with the Vesilind settling velocity (2.6), f_{bk} has a unique local maximum at $\hat{C} = 1/r_{\mathrm{V}}$.) In that case, after a straightforward systematic evaluation of (3.6) with all possible orderings of C_j, C_{j+1} and $\hat{C}$, the value of G_j can be computed by the following simple algorithm:

Algorithm 3.1 (Computation of G_j)**.**

Input: concentrations C_j and C_{j+1}, function f_{bk} with exactly one local maximum at $\hat{C}$

Output: value of G_j

if $C_j < C_{j+1}$ **then**

$G_j \leftarrow \min\{f_{\mathrm{bk}}(C_j), f_{\mathrm{bk}}(C_{j+1})\}$
else
  if $(\hat{C} - C_j) \cdot (\hat{C} - C_{j+1}) < 0$ **then**
    $G_j \leftarrow f_{\mathrm{bk}}(\hat{C})$
  else
    $G_j \leftarrow \max\{f_{\mathrm{bk}}(C_j), f_{\mathrm{bk}}(C_{j+1})\}$
  endif
endif

Summarizing, we obtain the following explicit formula for the numerical flux:

$$F_j^{\mathrm{num}} = F_j^{\mathrm{num}}(C_j, C_{j+1}, t) := \begin{cases} -(Q_{\mathrm{e}}(t)/A)C_{j+1} & \text{for } j = -2, -1, \\ -(Q_{\mathrm{e}}(t)/A)C_{j+1} + G_j & \text{for } j = 0, \ldots, j_{\mathrm{f}} - 1, \\ (Q_{\mathrm{u}}(t)/A)C_j + G_j & \text{for } j = j_{\mathrm{f}}, \ldots, N, \\ (Q_{\mathrm{u}}(t)/A)C_j & \text{for } j = N+1, N+2, \end{cases} \tag{3.7}$$

where G_j is given by (3.6) or Algorithm 3.1.

3.4. **Approximation of the dispersion and compression fluxes.** Using the shorter notation

$$d_{\mathrm{disp},j} := d_{\mathrm{disp}}\big(z_j, Q_{\mathrm{f}}(t)\big),$$

we approximate the dispersion flux (3.3) by a difference approximation

$$J_{\mathrm{disp}}(z_j, t) \approx J_{\mathrm{disp},j}^{\mathrm{num}} := d_{\mathrm{disp},j} \frac{C_{j+1} - C_j}{\Delta z}. \tag{3.8}$$

Analogously, we approximate the compression flux (3.4) as

$$J_{\mathrm{comp}}(z_j, t) \approx J_{\mathrm{comp},j}^{\mathrm{num}} := \gamma(z_j) \frac{D_{j+1}^{\mathrm{num}} - D_j^{\mathrm{num}}}{\Delta z}, \tag{3.9}$$

where D_j^{num} is either the exact or an approximate integrated compression coefficient (3.2). For some choices of the constitutive functions v_{hs} and σ_{e}, the primitive D of d_{comp} defined by (3.2) can be found as a closed-form expression (see, e.g., Bürger and Karlsen, 2001). Then we can simply define

$$D_j^{\mathrm{num}} := D(C_j) \qquad \text{(exact primitive)}.$$

If an exact primitive cannot be found, $D(C_j)$ has to be approximated by numerical integration. To obtain fast simulations, one can avoid calculating the quadrature in (3.2) at every time step during the simulation. This technique involves two steps. Before the simulation starts, use the trapezoidal rule to compute approximate values $\tilde{D}_i$ of $D(i\Delta C)$ on a finely discretized C-axis at the concentrations

$$C_{\mathrm{c}} + i\Delta C, \quad i = 0, 1, \ldots, M, \tag{3.10}$$

where $M\Delta C = C_{\max} - C_{\mathrm{c}}$ should hold, and where $C_{\max}$ is a chosen maximum concentration; see Section 3.7. During the simulation, we use linear interpolation to get the approximate value D_j^{num} of $D(C_j)$. This two-step procedure introduces an error, which depends on the

choice of ΔC or, equivalently, M. Without going into details, one should choose ΔC proportional to $(\Delta z)^{3/2}$ (M proportional to $N^{3/2}$) in order not to destroy the overall order of convergence when the approximation (3.9) is made. Since we are dealing with precomputations that do not influence the running simulation time, we reduce the error more by setting $M = N^2$. Furthermore, if $d_{\mathrm{comp}}(C)$ is discontinuous at $C = C_{\mathrm{c}}$, make sure that $d_{\mathrm{comp}}(C_{\mathrm{c}}) > 0$ in Algorithm 3.2; cf. (2.12).

Algorithm 3.2 (Precomputation of $\tilde{D}_i$)**.**

Inputs: number of layers N, critical concentration C_{c}, maximum concentration $C_{\max}$, function d_{comp}
Outputs: value ΔC, values $\tilde{D}_i$, $i = 0, 1, \ldots, M$
$M \leftarrow N^2$
$\Delta C \leftarrow (C_{\max} - C_{\mathrm{c}})/M$
$\tilde{D}_0 \leftarrow 0$
$d_0 \leftarrow d_{\mathrm{comp}}(C_{\mathrm{c}})$
for $i = 1, \ldots, M$
  $d_i \leftarrow d_{\mathrm{comp}}(C_{\mathrm{c}} + i\Delta C)$
  $\tilde{D}_i \leftarrow \tilde{D}_{i-1} + \frac{\Delta C}{2}(d_{i-1} + d_i)$
end

During the simulation, given a layer concentration $C_j > C_{\mathrm{c}}$, we use linear interpolation between $\tilde{D}_i$ and $\tilde{D}_{i+1}$ for a suitable index i to define D_j^{num}. This index i thus satisfies $C_{\mathrm{c}} + i\Delta C \le C_j < C_{\mathrm{c}} + (i+1)\Delta C$. The algorithm is the following, where $\lfloor x \rfloor$ is the nearest integer below the real number x.

Algorithm 3.3 (Computation of D_j^{num})**.**

Inputs: values j, ΔC, C_j and $\tilde{D}_i$, $i = 0, 1, \ldots, M$
Output: value D_j^{num}
if $C_j \le C_{\mathrm{c}}$
  $D_j^{\mathrm{num}} \leftarrow 0$
else
  $i \leftarrow \lfloor (C_j - C_{\mathrm{c}})/\Delta C \rfloor$
  $D_j^{\mathrm{num}} \leftarrow \left(\dfrac{C_j}{\Delta C} - i\right)\tilde{D}_{i+1} + \left(i + 1 - \dfrac{C_j}{\Delta C}\right)\tilde{D}_i$
end

3.5. **Method of lines.** The feed term in the last line of (3.5) can be handled directly; we just add $Q_{\mathrm{f}}(t)C_{\mathrm{f}}(t)/(A\Delta z)$ to the right-hand side of the equation for $j = j_{\mathrm{f}}$. Consequently, we obtain the method-of-lines formula

$$\begin{aligned}\frac{\mathrm{d}C_j}{\mathrm{d}t} = &-\frac{F_j^{\mathrm{num}} - F_{j-1}^{\mathrm{num}}}{\Delta z} \\ &+ \frac{1}{\Delta z}\Big(J_{\mathrm{disp},j}^{\mathrm{num}} - J_{\mathrm{disp},j-1}^{\mathrm{num}} + J_{\mathrm{comp},j}^{\mathrm{num}} - J_{\mathrm{comp},j-1}^{\mathrm{num}}\Big) \\ &+ \frac{Q_{\mathrm{f}}C_{\mathrm{f}}}{A\Delta z}\delta_{j,j_{\mathrm{f}}}, \qquad j = -1, \ldots, N+2,\end{aligned} \tag{3.11}$$

where δ_{j,j_f} is the standard Kronecker symbol with $\delta_{j,j_\mathrm{f}} = 1$ if $j = j_\mathrm{f}$ and $\delta_{j,j_\mathrm{f}} = 0$ otherwise. (Recall that $j = -1$ and $j = 0$ correspond to the layers of the effluent zone, $[z_{-2}, z_{-1}]$ and $[z_{-1}, z_0]$.) The expressions F_j^{num}, $J_{\mathrm{disp},j}^{\mathrm{num}}$ and $J_{\mathrm{comp},j}^{\mathrm{num}}$ are defined by (3.7), (3.8) and (3.9), respectively. Formula (3.11) is an approximation of the exact conservation law formulation (3.5).

Note that not all of the terms in (3.11) are present in every layer. Explicitly, we obtain for the layer with $j = -1$ completely located in the effluent zone:

$$\frac{\mathrm{d}C_{-1}}{\mathrm{d}t} = \frac{Q_\mathrm{e}}{A\Delta z}(C_0 - C_{-1}), \tag{3.12}$$

for the layer with $j = 0$ in the effluent zone adjacent to the effluent level $z_0 = -H$:

$$\frac{\mathrm{d}C_0}{\mathrm{d}t} = \frac{Q_\mathrm{e}}{A\Delta z}(C_1 - C_0) - \frac{G_0}{\Delta z} + \frac{D_1^{\mathrm{num}} - D_0^{\mathrm{num}}}{(\Delta z)^2}, \tag{3.13}$$

for layer 1 within the SST:

$$\begin{aligned}\frac{\mathrm{d}C_1}{\mathrm{d}t} = {} & \frac{Q_\mathrm{e}}{A\Delta z}(C_2 - C_1) - \frac{G_1 - G_0}{\Delta z} \\ & + \frac{1}{(\Delta z)^2}\Big(d_{\mathrm{disp},1}(C_2 - C_1) \\ & + D_2^{\mathrm{num}} - 2D_1^{\mathrm{num}} + D_0^{\mathrm{num}}\Big),\end{aligned} \tag{3.14}$$

for layers $j = 2, \ldots, j_\mathrm{f} - 1$:

$$\begin{aligned}\frac{\mathrm{d}C_j}{\mathrm{d}t} = {} & \frac{Q_\mathrm{e}}{A\Delta z}(C_{j+1} - C_j) - \frac{G_j - G_{j-1}}{\Delta z} \\ & + \frac{1}{(\Delta z)^2}\Big(d_{\mathrm{disp},j}(C_{j+1} - C_j) - d_{\mathrm{disp},j-1}(C_j - C_{j-1}) \\ & + D_{j+1}^{\mathrm{num}} - 2D_j^{\mathrm{num}} + D_{j-1}^{\mathrm{num}}\Big),\end{aligned} \tag{3.15}$$

for the feed layer $j = j_\mathrm{f}$:

$$\begin{aligned}\frac{\mathrm{d}C_{j_\mathrm{f}}}{\mathrm{d}t} = {} & -\frac{Q_\mathrm{u} + Q_\mathrm{e}}{A\Delta z}C_{j_\mathrm{f}} - \frac{G_{j_\mathrm{f}} - G_{j_\mathrm{f}-1}}{\Delta z} \\ & + \frac{1}{(\Delta z)^2}\Big(d_{\mathrm{disp},j_\mathrm{f}}(C_{j_\mathrm{f}+1} - C_{j_\mathrm{f}}) - d_{\mathrm{disp},j_\mathrm{f}-1}(C_{j_\mathrm{f}} - C_{j_\mathrm{f}-1}) \\ & + D_{j_\mathrm{f}+1}^{\mathrm{num}} - 2D_{j_\mathrm{f}}^{\mathrm{num}} + D_{j_\mathrm{f}-1}^{\mathrm{num}}\Big) \\ & + \frac{Q_\mathrm{f}C_\mathrm{f}}{A\Delta z},\end{aligned} \tag{3.16}$$

for the layers with $j = j_\mathrm{f}+1, \dots, N-1$ in the thickening zone:

$$\begin{aligned}\frac{\mathrm{d}C_j}{\mathrm{d}t} &= -\frac{Q_\mathrm{u}}{A\Delta z}(C_j - C_{j-1}) - \frac{G_j - G_{j-1}}{\Delta z} \\ &\quad + \frac{1}{(\Delta z)^2}\Big(d_{\mathrm{disp},j}(C_{j+1} - C_j) - d_{\mathrm{disp},j-1}(C_j - C_{j-1}) \\ &\quad + D_{j+1}^\mathrm{num} - 2D_j^\mathrm{num} + D_{j-1}^\mathrm{num}\Big),\end{aligned} \tag{3.17}$$

for the bottom layer in the thickening zone:

$$\begin{aligned}\frac{\mathrm{d}C_N}{\mathrm{d}t} &= -\frac{Q_\mathrm{u}}{A\Delta z}(C_N - C_{N-1}) - \frac{G_N - G_{N-1}}{\Delta z} \\ &\quad + \frac{1}{(\Delta z)^2}\Big(-d_{\mathrm{disp},N-1}(C_N - C_{N-1}) \\ &\quad + D_{N+1}^\mathrm{num} - 2D_N^\mathrm{num} + D_{N-1}^\mathrm{num}\Big),\end{aligned} \tag{3.18}$$

for the two layers that form the underflow zone:

$$\frac{\mathrm{d}C_{N+1}}{\mathrm{d}t} = -\frac{Q_\mathrm{u}}{A\Delta z}(C_{N+1} - C_N) + \frac{G_N}{\Delta z} - \frac{D_{N+1}^\mathrm{num} - D_N^\mathrm{num}}{(\Delta z)^2}, \tag{3.19}$$

and

$$\frac{\mathrm{d}C_{N+2}}{\mathrm{d}t} = -\frac{Q_\mathrm{u}}{A\Delta z}(C_{N+2} - C_{N+1}). \tag{3.20}$$

3.6. **Time discretization.** The method-of-lines equations (3.12)–(3.20) can be implemented when solvers for the layer-wise defined ODEs are available. This is particularly handy when the SST should be simulated together with several other ODEs modelling the biological reactors of an activated sludge process. However, since the spatial accuracy of the scheme is only of first order, there is probably not much to gain in terms of speed by using any high-order-in-time ODE solver. A simple explicit Eulerian time step is sufficient. To this end we select a time step $\Delta t > 0$ according to the CFL (Courant-Friedrichs-Lewy) condition; see Section 3.7, and let $t_n := n\Delta t$. We denote by C_j^n the value of the layer concentration at time t_n, cf. (3.1),

$$C_j^n := C_j(t_n) = \frac{1}{\Delta z}\int_{z_{j-1}}^{z_j} C(z, t_n)\,\mathrm{d}z,$$
$$j = -1, \dots, N+2, \quad n = 0, 1, 2, \dots.$$

In the method-of-lines ODEs (3.12)–(3.20), we approximate the time derivative by the explicit Euler step

$$\frac{\mathrm{d}C_j}{\mathrm{d}t}(t_n) \approx \frac{C_j^{n+1} - C_j^n}{\Delta t},$$

evaluate the right-hand side of (3.11) at $t = t_n$ and replace $C_j(t_n)$ by C_j^n. Multiplying the resulting equation by Δt, adding C_j^n to both sides we obtain the fully discrete method

$$\begin{aligned} C_j^{n+1} = C_j^n &- \frac{\Delta t}{\Delta z}\Big(F_j^{\mathrm{num},n} - F_{j-1}^{\mathrm{num},n}\Big) \\ &+ \frac{\Delta t}{\Delta z}\Big(J_{\mathrm{disp},j}^{\mathrm{num},n} - J_{\mathrm{disp},j-1}^{\mathrm{num},n} + J_{\mathrm{comp},j}^{\mathrm{num},n} - J_{\mathrm{comp},j-1}^{\mathrm{num},n}\Big) \\ &+ \frac{\Delta t}{\Delta z}\frac{Q_{\mathrm{f}}(t_n)C_{\mathrm{f}}(t_n)}{A}\delta_{j,j_{\mathrm{f}}}, \qquad j = -1, \ldots, j = N+2, \end{aligned} \tag{3.21}$$

where $F_j^{\mathrm{num},n} := F_j^{\mathrm{num}}(C_j, C_{j+1}, t_n)$, etc. We leave to the reader to write out this algorithm for each layer.

3.7. **CFL condition.** Suppose that we want to use the fully discrete method (3.21) to simulate an SST over a time interval $[0, T]$. Given the chosen layer depth Δz, the time step Δt must be chosen such that the following condition is satisfied:

$$\begin{aligned} \Delta t \leq \Bigg[&\frac{1}{\Delta z}\left(\max_{0\leq t\leq T}\frac{Q_{\mathrm{f}}(t)}{A} + \max_{0\leq C\leq C_{\max}}\big|f_{\mathrm{bk}}'(C)\big|\right) \\ &+ \frac{2}{(\Delta z)^2}\left(\max_{0\leq C\leq C_{\max}} d_{\mathrm{comp}}(C) + \max_{\substack{-H\leq z\leq B,\\ 0\leq t\leq T}} d_{\mathrm{disp}}\big(z, Q_{\mathrm{f}}(t)\big)\right)\Bigg]^{-1}. \end{aligned} \tag{3.22}$$

Observe that for a given spatial discretization Δz, inequality (3.22) yields an upper limit of the time step Δt that must be submitted into any ODE solver for the method-of-lines equations (3.11). A condition like (3.22) is known in numerical analysis as a "CFL condition". It is a necessary condition to ensure stability of the numerical scheme. For computational purposes, the maximum concentration $C_{\max}$ should be set to a sufficiently large value (above C_{c}), where the function value and derivative of f_{bk} is almost zero. Then $d_{\mathrm{comp}}(C)$ is also small. Whether $C_{\max}$ is set to, for example, 20 or 30 kg/m^3 has no impact on the simulation time.

4. How to convert the Takács method to a reliable one

4.1. **Upgrade the numerical flux.** The simulation method by Takács et al. (1991) is implemented in many simulators for the SST. The method is roughly the one by Vitasovic (1989) with the specific constitutive relation given by the double exponential settling velocity function (2.7). The key ingredient is, however, the numerical flux update, which comes from Stenstrom (1976):

$$S_j = \min\big\{f_{\mathrm{bk}}(C_j), f_{\mathrm{bk}}(C_{j+1})\big\}. \tag{4.1}$$

This expression should be compared with the Godunov flux G_j in (3.6), which contains a minimum function, however over an entire interval instead of only at the two concentration values C_j and C_{j+1}. When the function f_{bk} has precisely one local maximum (which is the only realistic case known to the authors), the computation of Godunov's flux can be done by Algorithm 3.1. In this algorithm, (4.1) can be found in the first if-then statement. Hence,

Stenstrom' flux (4.1) can easily be upgraded to the reliable Godunov flux by adding a few more lines in the simulation program.

A fundamental principle for any consistent modelling methodology (Bürger et al., 2011), is that all model parameters should be included in the physical constitutive assumptions only, so that they appear in the model PDE and then are carried over to any numerical method. No parameters should be introduced in the numerical algorithm itself. Consequently, the threshold parameter in the clarification zone layers in Takács' model should be removed.

4.2. **Upgrade the outlet concentrations.** The Takács method assumes that the concentration in the top layer is the same as the one in the effluent. In some situations, this is an unphysical assumption which the present simulation method avoids. The physically correct approach is that the conservation of mass should hold also across the outlets, i.e., the flux of particles leaving the top layer should be equal to what the effluent pipe receives. The effluent concentration is a part of the solution of the model equation (1.1), namely in $z < -H$. (The analogous situation holds at the bottom of the SST.) Recall that the assumption is that there is only bulk transport (neither settling, compression nor dispersion) outside the SST; cf. (2.3). In the numerical method, correct outlet concentrations are automatically obtained by means of the extra layers outside the SST.

4.3. **Add compression and dispersion effects.** To be able to calculate approximations of the second-order spatial derivative effects, two extra layers have to be added at the top and bottom, respectively, outside the SST. The dispersion flux (3.8) is straightforwardly included when a constitutive relation for $d_{\mathrm{disp}}(z, Q_{\mathrm{f}})$ has been chosen.

The compression flux needs some more care to include, and there are in addition pitfalls; see Bürger et al. (2012). Once a constitutive function for d_{comp} has been chosen, it is important to first find the primitive of this, which often has to be done numerically with the precomputation in Algorithm 3.2.

4.4. **Implement the CFL condition.** After an implementation of the CFL condition (3.22), the method-of-lines formulas in Section 3.5 or the fully discrete method in Section 3.6 can be used.

5. Simulations

A demonstration of the possibilities of turning on and off the optional effects of compression and dispersion with the proposed method has already been presented by Bürger et al. (2011). Here, we investigate further the effect of dispersion on the outlet concentrations and on the transient behaviour between different steady states. For a detailed comparison with a proved reliable numerical method as well as discussions on pitfalls and comparisons with other simulation models, we refer to Bürger et al. (2012). In that paper and here we use the same constitutive functions v_{hs}, σ_{e} and d_{disp}, namely the Vesilind settling velocity (2.6), the logarithmic effective solids stress function (2.10) and the exponential dispersion function (2.14). This implies that the function d_{comp} is given by (2.12). For the constants in those functions, we set $v_0 = 3.47\,\mathrm{m/h}$, $r_{\mathrm{V}} = 0.37\,\mathrm{m^3/kg}$, $\alpha = 4.00\,\mathrm{Pa}$, $\beta = 4.00\,\mathrm{kg/m^3}$, $\rho_{\mathrm{s}} = 1050\,\mathrm{kg/m^3}$, $\Delta\rho = 52\,\mathrm{kg/m^3}$, $g = 9.81\,\mathrm{m/s^2}$ and $C_{\mathrm{c}} = 6.00\,\mathrm{kg/m^3}$. The constants α_1 and α_2 in the dispersion function (2.14), will be varied to illustrate their respective effect. The

maximum concentration for the CFL condition (3.22) is chosen as $C_{\max} = 20\,\mathrm{kg/m^3}$. We consider an SST with $H = 1$ m, $B = 3$ m and $A = 400$ m^2, and let the number of internal layers (within the SST) be $N = 90$ (i.e. a total of 94 layers for the numerical method).

In the first three simulations the volumetric flows are kept constant: $Q_{\mathrm{f}}(t) = 250\,\mathrm{m^3/h}$, $Q_{\mathrm{u}}(t) = 80\,\mathrm{m^3/h}$, and hence $Q_{\mathrm{e}}(t) = 170\,\mathrm{m^3/h}$ for $0 \le t \le 800$ h. The feed concentration is chosen as

$$C_{\mathrm{f}}(t) = \begin{cases} 4.0\ \mathrm{kg/m^3}, & 0 \le t < 50\ \mathrm{h}, \\ 3.7\ \mathrm{kg/m^3}, & 50 \le t < 250\ \mathrm{h}, \\ 4.1\ \mathrm{kg/m^3}, & 250 \le t < 800\ \mathrm{h}. \end{cases}$$

The SST is initially in a steady state with a sludge blanket level at the depth 0.6 m obtained from a simulation without dispersion, i.e. $\alpha_1 = 0\,\mathrm{m^{-1}}$, and with $C_{\mathrm{f}} = 4.0\ \mathrm{kg/m^3}$.

To illustrate the CFL condition (3.22), we get the following for Simulations 2 and 3 (where all effects are included):

$$\Delta t \le \left[\frac{4.0972\ \mathrm{m/h}}{\Delta z} + \frac{1.5525\ \mathrm{m^2/h}}{(\Delta z)^2} \right]^{-1}.$$

Since $\Delta z = (4\ \mathrm{m})/N$, we get for $N = 90$: $\Delta z = 0.0444$ m ≈ 4 cm and $\Delta t \le 0.00114$ h ≈ 4 s, which is reasonable for this type of spatial detail. A more detailed investigation of this condition is beyond the scope of this paper.

Simulation 1, no dispersion. When $\alpha_1 = 0\,\mathrm{m^{-1}}$ there is no dispersion. The simulation shown in Figure 3a shows that the initial steady state is kept the first 50 hours and the other two steady states some time after the change in the feed concentration. The third (and final) steady state ($C_{\mathrm{f}} = 4.1$) has a sludge blanket level slightly higher in the SST and the underflow concentration is higher than in the initial state ($C_{\mathrm{f}} = 4.0$). During the entire simulation, a discontinuity can be noticed at the feed level.

Simulation 2, dispersion in $|z| < 0.4$ m. We now introduce some dispersion around the inlet by setting $\alpha_1 = 0.001\,\mathrm{m^{-1}}$ and $\alpha_2 = 0.0016\,\mathrm{h/m^2}$, which means that $\alpha_2 Q_{\mathrm{f}} = 0.4$ m is the distance from the inlet where dispersion is present; see Figure 3b. The (previous) discontinuity at the feed level is now smoothed. In the first part of the simulation where the sludge blanket is quite low, no effect different from Figure 3a can be observed. After about 300 hours when the sludge blanket rises up into the region of dispersion, the solution is clearly smoothed and the sludge blanket rises up into the clarification zone.

Simulation 3, dispersion in $|z| < 0.8$ m. With $\alpha_1 = 0.001\,\mathrm{m^{-1}}$ and $\alpha_2 = 0.0032\,\mathrm{h/m^2}$, the region of dispersion is now doubled; $\alpha_2 Q_{\mathrm{f}} = 0.8$ m. As Figure 3c shows, the initial steady state is smoothed slightly, since the location of the initial sludge blanket is $z = 0.6 < 0.8$ m. As in Figure 3b, the third steady state contains a sludge blanket in the clarification zone but now at a higher level. Thus, the more dispersion, the more total sludge mass in the SST at steady state. This is clearly seen in Figure 3d, where the concentration profiles of Simulations 1 and 3 at the end time $t = 800$ h are shown. The effluent concentration is $C_{\mathrm{e}}(t) = 0$ for $0 \le t \le 800$ h for all three simulations. In the final steady state, the underflow concentration C_{u} is therefore uniquely determined by the feed mass flow via the steady-state

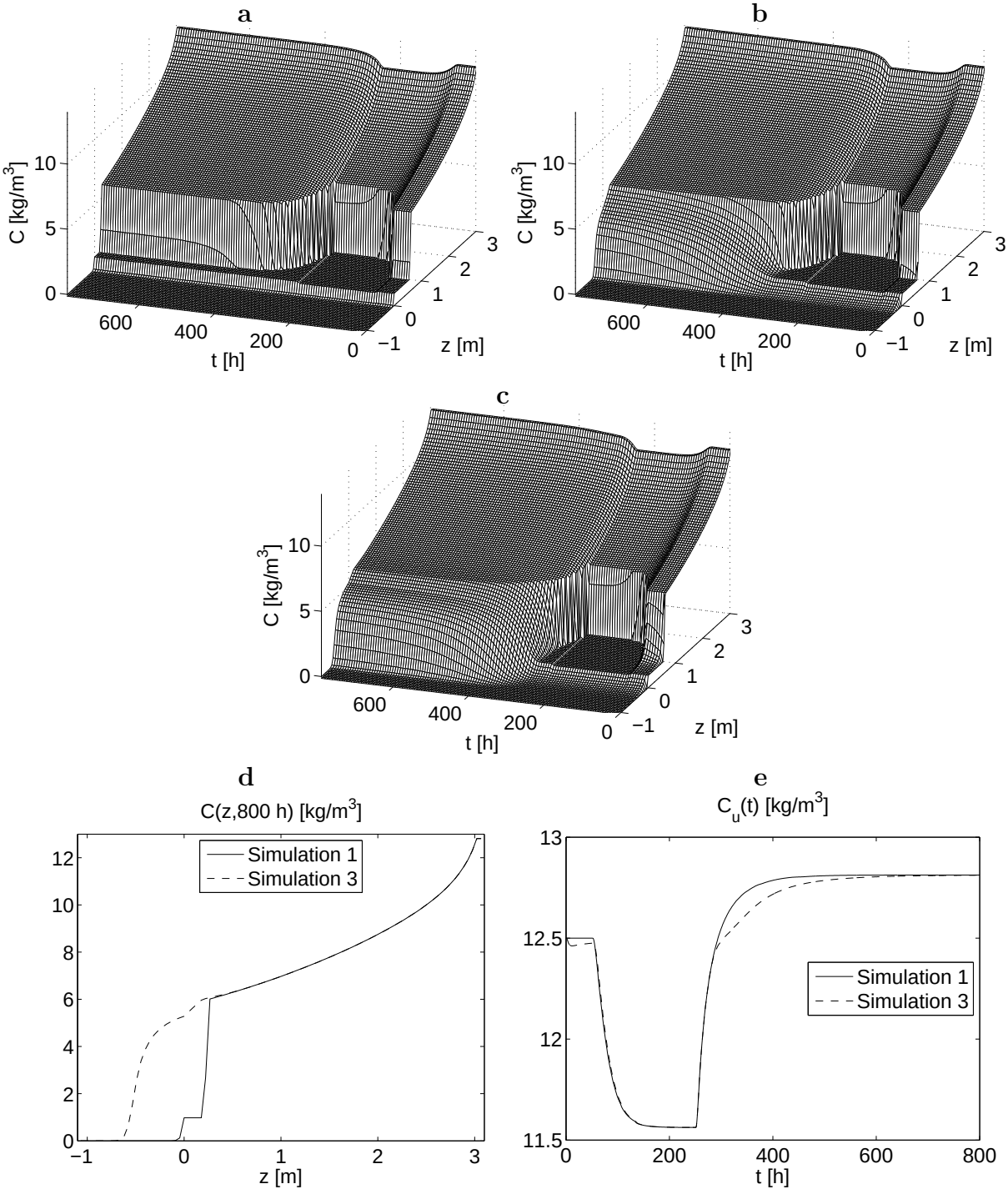

FIGURE 3. Three simulations of the same scenario (a-c) with different amount of dispersion. The last two plots show details of Simulations 1 and 3.

mass balance $Q_{\mathrm{f}}C_{\mathrm{f}} = Q_{\mathrm{u}}C_{\mathrm{u}}$. Given C_{u}, the steady-state profile is uniquely given by the solution of an ODE; see Bürger and Narváez (2007). Consequently, the steady-state profiles

for Simulations 1 and 3 are the same from the bottom up to $z = -0.8$ m, above which there is dispersion in Simulation 3; see Figure 3d. As Figure 3e shows, the difference in the underflow concentration during transients explains the difference in mass in the final steady states.

Simulation 4, higher Q_{f}, no dispersion. We apply the same conditions as in Simulation 1, except for the feed volumetric flow, which is now increased to $Q_{\mathrm{f}} = 270\,\mathrm{m}^3/\mathrm{h}$. Figure 4a shows a transient with the sludge blanket rising up into the clarification zone. As $C_{\mathrm{f}} = 3.7$ kg/m^3, an almost stationary sludge blanket at about $z = 0.6$ m appears before $t = 250$ h. In the final steady state, the clarification zone is filled with sludge and the flocs are moving only slowly upwards since the bulk flow upwards (Q_{e}/A) is only slightly higher than the settling velocity downwards. Hence, only a small amount of sludge is actually leaving through the effluent at the concentration $C_{\mathrm{e}}(800\text{ h}) = 358$ mg/l. Thus, this is an example of a discontinuity arising at the effluent level. The underflow concentration is $C_{\mathrm{u}}(800\text{ h}) = 12.99$ kg/m^3 and the steady-state mass conservation is fulfilled:

$$Q_{\mathrm{u}}C_{\mathrm{u}} + Q_{\mathrm{e}}C_{\mathrm{e}} = 1038.94 + 68.06 = 1107.00 = Q_{\mathrm{f}}C_{\mathrm{f}} \qquad [\mathrm{kg/h}].$$

Simulation 5, higher Q_{f}, dispersion in $|z| < 0.8$ m. The same conditions as in Simulation 4 are used, but with $\alpha_1 = 0.001\,\mathrm{m}^{-1}$ and $\alpha_2 = 0.8/270\,\mathrm{h/m}^2$, which implies that the region of dispersion is $|z| \le \alpha_2 Q_{\mathrm{f}} = 0.8$ m; see Figure 4b. In the final steady state there is a higher effluent concentration, $C_{\mathrm{e}}(800\text{ h}) = 419$ mg/l, than in Simulation 4. This is an increase of 17% for the same feed load. The dispersion term can thus be used to simulate SSTs that are identical except for different inlet works. To date, we have not seen this feature in literature. This opens perspectives to include other processes such as flocculation. The underflow concentration $C_{\mathrm{u}}(800\text{ h}) = 12.84$ kg/m^3 is lower than in Simulation 4; see Figure 4c. The steady-state mass conservation is again satisfied:

$$Q_{\mathrm{u}}C_{\mathrm{u}} + Q_{\mathrm{e}}C_{\mathrm{e}} = 1027.44 + 79.56 = 1107.00 = Q_{\mathrm{f}}C_{\mathrm{f}} \qquad [\mathrm{kg/h}]$$

Note that the mass flow through the effluent is higher, $79.56 - 68.06 = 11.50$ kg/h, with dispersion than without. The different underflow concentrations during Simulations 4 and 5 are shown in Figure 4d.

6. Conclusions

The derivation and implementation of a numerical method for 1D simulation of SSTs is presented. The simulation method has the following features:

- It is derived from the conservation law of mass supported by PDE theory and adherent numerical analysis. No heuristic parameters are introduced in the numerical method and no assumptions on the solution are made; e.g. the concentration is continuous over the outlets. In Simulation 4, we have demonstrated that there may be a concentration discontinuity at the effluent level as part of the solution.
- It is reliable in the sense that it produces correct numerical approximations of the exact solution of the model PDE. This means that it is also robust, since it can handle all possible situations and choices of number of layers. Necessary ingredients

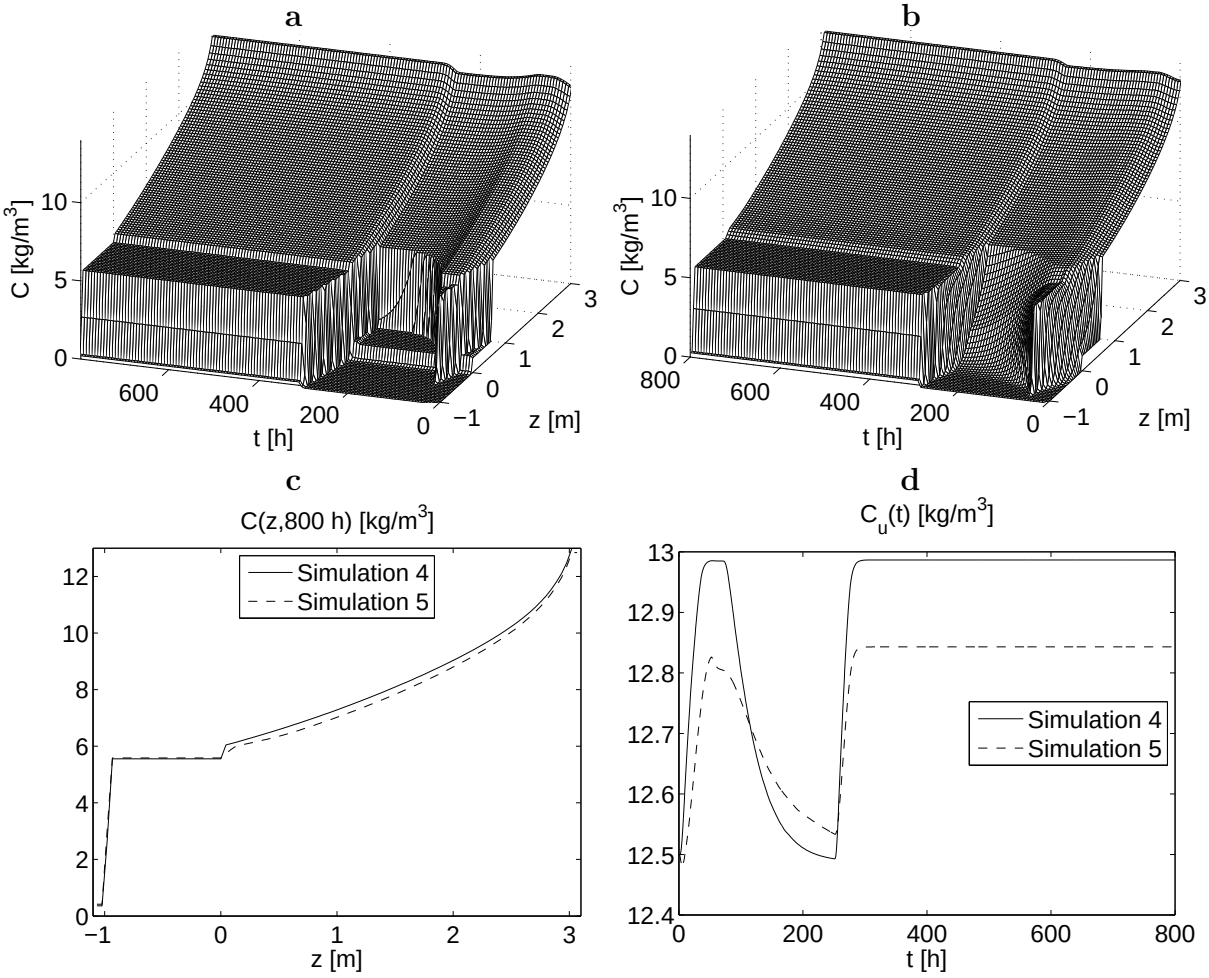

FIGURE 4. Simulations 4 and 5 show an overloaded situation without dispersion (a) and with (b).

are the extra layers outside the SST, the time step limitation (CFL condition) and careful discretizations of the convection and compression terms.

- According to consistent modelling methodology, all model parameters are introduced only in the physical constitutive relations, which comprise hindered sedimentation, compression of particles at high concentrations and dispersion that depends on depth and volumetric feed flow.
- It is more general than previously published 1D simulation methods, since reliable simulations are obtained irrespective of whether the modelling phenomena of compression and dispersion are turned on or off, separately.
- Simulations indicate that although dispersion is localized around the inlet, it influences all concentrations in the SST during transient situations and in overloaded steady states. In other steady states ($C_e = 0$), dispersion around the inlet only influences the concentrations locally, so that the underflow concentration is not influenced. However, the total sludge mass in the SST is increased.

- The physically correct Godunov numerical flux is computed in a fast and simple way (Algorithm 3.1). This flux can be seen as a direct extension of the well-known Stenstrom-Vitasovic-Takács flux.
- The Takács simulation model, which has served the community for over 20 years and still is in use in many commercial simulators, can now fairly easily be upgraded to the presented reliable simulation model, which includes additional effects that can be customarily chosen.

Acknowledgements

RB acknowledges partial support by Fondecyt project 1090456, and BASAL project CMM, Universidad de Chile and Centro de Investigación en Ingeniería Matemática (CI^{2}MA), Universidad de Concepción. SD acknowledges support by the Foundation for Engineering Scientific Research to the Memory of J. Gust. Richert, SWECO AB, Sweden. SF acknowledges support by the Crafoord Foundation, Sweden (grant 20110535). IN and ET thank the Flemish Fund for Scientific Research (Project G.A051.10).

References

Abusam, A., Keesman, K.J., 2009. Dynamic modeling of sludge compaction and consolidation processes in wastewater secondary settling tanks. Water Environ. Res. 81 (1), 51–56.

Anderson, H.M. and Edwards, R.V., 1981. A finite difference scheme for the simulation of continuous sedimentation. AIChE Symposium Ser. 77 (209), 227–238

Attir, U., Denn, M.M., 1978. Dynamics and control of the activated sludge wastewater process. AIChE J. 24, 693–698.

Bürger, R., Diehl, S., Nopens, I., 2011. A consistent modelling methodology for secondary settling tanks in wastewater treatment. Water Res. 45, 2247–2260.

Bürger, R., Diehl, S., Farås, S. and Nopens, I., 2012. Simulation of the secondary settling process with reliable numerical methods. Submitted, available at http://www.ci2ma.udec.cl/publicaciones/prepublicaciones/index.php

Bürger, R., Karlsen, K.H., 2001. On some upwind schemes for the phenomenological sedimentation-consolidation model. J. Eng. Math. 41, 145–166.

Bürger, R., Karlsen, K.H., Torres, H., Towers, J.D., 2010. Second-order schemes for conservation laws with discontinuous flux modelling clarifier-thickener units. Numer. Math. 116, 579–617.

Bürger, R., Karlsen, K.H., Towers, J.D., 2005. A model of continuous sedimentation of flocculated suspensions in clarifier-thickener units. SIAM J. Appl. Math. 65, 882–940.

Bürger, R., Narváez, A., 2007. Steady-state, control, and capacity calculations for flocculated suspensions in clarifier-thickeners. Int. J. Mineral Process. 84, 274–298.

Cacossa, K.F., Vaccari, D.A., 1994. Calibration of a compressive gravity thickening model from a single batch settling curve. Water Sci. Tech., 30, 107–116.

Chancelier, J.P., Cohen de Lara, M., Joannis, C., Pacard, F., 1997. New insights in dynamic modeling of a secondary settler — II. Dynamical analysis. Wat. Res. 31, 1857–1866.

Chatellier, P., Audic, J.M., 2000. A new model for wastewater treatment plant clarifier simulation. Wat. Res. 34, 690–693.

David, R., Saucez, P., Vasel, J.-L., Vande Wouwer, A., 2009a. Modeling and numerical simulation of secondary settlers: a method of lines strategy. Water Res. 43 (2), 319–330.

David, R., Vasel, J.-L., Vande Wouwer, A., 2009b. Settler dynamic modeling and MATLAB simulation of the activated sludge process. Chem. Eng. J. 146, 174–183.

De Clercq, J., Devisscher, M., Boonen, I., Vanrolleghem, P.A., Defrancq, J., 2003. A new one-dimensional clarifier model — verification using full-scale experimental data. Wat. Sci. Tech. 47 (12), 105–112.

De Clercq, J., Devisscher, M., Boonen, I., Defrancq, J., Vanrolleghem, P.A., 2005a. Analysis and simulation of the sludge profile dynamics in a full-scale clarifier. J. Chem. Technol. Biotechnol. 80, 523–530.

De Clercq, J., Jacobs, F., Kinnear, D.J., Nopens, I., Dierckx, R.A., Defrancq, J., Vanrolleghem, P.A., 2005b. Detailed spatio-temporal solids concentration profiling during batch settling of activated sludge using a radiotracer. Wat. Res. 39, 2125–2135.

De Clercq, J., Nopens, I., Defrancq, J., Vanrolleghem, P.A., 2008. Extending and calibrating a mechanistic hindered and compression settling model for activated sludge using in-depth batch experiments. Water Res. 42, 781–791.

Diehl, S., 1996. A conservation law with point source and discontinuous flux function modelling continuous sedimentation. SIAM J. Appl. Math. 56, 388–419.

Diehl, S., 2000. On boundary conditions and solutions for ideal clarifier-thickener units. Chem. Eng. J. 80, 119–133.

Diehl, S., 2008. The solids-flux theory — confirmation and extension by using partial differential equations. Water Res. 42 (20), 4976–4988.

Diehl, S., Jeppsson, U., 1998. A model of the settler coupled to the biological reactor. Water Res. 32 (2), 331–342.

Engquist, B., Osher, S., 1981. One-sided difference approximations for nonlinear conservation laws. Math. Comp. 36, 321–351.

Giokas, D.L., Kim, Y., Paraskevas, P.A., Paleologos, E.K., Lekkas, T.D. (2002) A simple empirical model for activated sludge thickening in secondary clarifiers, Wat. Res. 36, 3245–3252.

Godunov, S.K., 1959. Finite difference methods for numerical computation of discontinuous solutions of equations of fluid dynamics. Mat. Sb. 47, 271–295 (in Russian).

Guo, Y., Hu, Y. and Li, B., 2010. Application analysis of one-dimensional sedimentation model. IEEE Xplore paper, Fourth International Conference on Bioinformatics and Biomedical Engineering, Chengdu, China, June, 18–20.

Härtel, L. and Pöpel, H.J., 1992. A dynamic secondary clarifier model including processes of sludge thickening. Wat. Sci. Tech. 25, no. 6, 267–284.

Jeppson, U., Diehl, S., 1996a. An evaluation of a dynamic model of the secondary clarifier. Wat. Sci. Tech. 34, no. 5–6, 19–26.

Jeppson, U., Diehl, S., 1996b. On the modelling of the dynamic propagation of biological components in the secondary clarifier. Wat. Sci. Tech. 34, no. 5–6, 85–92.

Koehne, M., Hoen, K., Schuhen, M., 1995. Modelling and simulation of final clarifiers in wastewater treatment plants. Math. Comput. Simul 39 (5–6), 609–616.

Kynch, G.J., 1952. A theory of sedimentation. Trans. Farad. Soc. 48, 166–176.

Lee, T.T., Wang, F.Y., Newell, R.B., 2006. Advances in distributed parameter approach to the dynamics and control of activated sludge processes for wastewater treatment. Water Res. 40 (5), 853–869.

Lev, O., Rubin, E., Sheintuch, M., 1986. Steady state analysis of a continuous clarifier-thickener system, AIChE J. 32, 1516–1525.

Martin, A.D., 2004. Optimisation of clarifier-thickeners processing stable suspensions for turn-up/turn

Otterpohl, R., Freund, M., 1992. Dynamic models for clarifiers of activated sludge plants with dry and wet weather flows. Wat. Sci. Tech. 26, no. 5–6, 1391–1400.

Plósz, B.G., Weiss, M., Printemps, C., Essemiani, K., Meinhold, J., 2007. One-dimensional modelling of the secondary clarifier — factors affecting simulation in the clarification zone and the assessment of the thickening flow dependence. Wat. Res. 41, 3359–3371.

Plósz, B.G., Nopens, I., DeClercq, J., Benedetti, L., Vanrolleghem, P.A. 2011. Shall we upgrade one-dimensional secondary settler models used in WWTP simulators? An assessment of model structure uncertainty and its propagation. Water Sci. Tech. 63(8), 1726-1738.

Queinnec, I., Dochain, D., 2001. Modelling and simulation of the steady-state of secondary settlers in wastewater treatment plants. Water Sci. Tech. 43 (7), 39–46.

Stenstrom, M.K., 1976. A dynamic model and computer compatible control strategies for wastewater treatment plants. PhD dissertation, Clemson University, Clemson, South Carolina, USA.

Takács, I., Patry, G.G., Nolasco, D., 1991. A dynamic model of the clarification-thickening process. Wat. Res. 25, 1263–1271.

Tiller, F.M., Leu, W.F., 1980. Basic data fitting in filtration. J. Chin. Inst. Chem. Engrs. 11, 61–70.

Vaccari, D.A., Uchrin, C.G., 1989, Modeling and simulation of compressive gravity thickening of activated sludge. J. Environ. Sci. Health, A24 (6), 645–674.

Verdickt, L., Smets, I., Van Impe, J., 2005. Sensitivity analysis of a one-dimensional convection-diffusion model for secondary settling tanks. Chem. Eng. Commun. 192, 1567–1585.

Vesilind, P.A., 1968. Design of prototype thickeners from batch settling tests. Water Sewage Works 115, 302–307.

Vitasovic, Z., 1989. Continuous settler operation; a dynamic model. In: Patry, G.G., Chapman, D. (Eds), Dynamic Modeling and Expert Systems in Wastewater Engineering, Lewis Publishers, Chelsea, MI, 59–81.

Watts, R.W., Svoronos, S.A., Koopman, B., 1996. One-dimensional modeling of secondary clarifiers using a concentration and feed velocity-dependent dispersion coefficient. Wat. Res. 30, 2112–2124.

Wett, B., 2002. A straight interpretation of the solids flux theory for a three-layer sedimentation model. Wat. Res. 36, 2949–2958.